Journal of Power Sources 228 (2013) 120–131

Contents lists available at SciVerse ScienceDirect

Journal of Power Sources

journal homepage: www.elsevier.com/locate/jpowsour

Exploring the cycle behavior of electrodeposited vanadium oxide electrochemical capacitor electrodes in various aqueous environments

A.M. Engstrom, F.M. Doyle*

Department of Materials Science and Engineering, 210 Hearst Mining Building, University of California, Berkeley, CA 94720 1760, USA

HIGHLIGHTS

- Electrodeposited vanadium oxide films were tested in multiple aqueous environments.
- The morphology is pH-dependent and does not exhibit smoothing upon cycling.
- Material dissolution is the primary cause of capacitive degradation upon cycling.
- The dissolved species are determined for each pH environment tested.

GRAPHICAL ABSTRACT

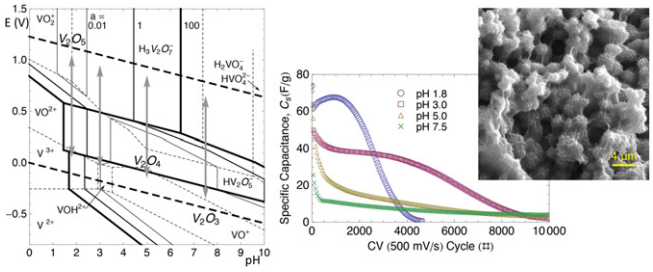

ARTICLE INFO

Article history:
Received 19 August 2012
Received in revised form
19 November 2012
Accepted 21 November 2012
Available online 29 November 2012

Keywords:
Vanadium oxide
Electrodeposition
Electrochemical capacitor
Cycle behavior
Degradation

ABSTRACT

Electrodeposited vanadium oxide has emerged as a potential electrochemical capacitor material due to its attractive initial pseudocapacitive performance. However, it suffers from capacitive degradation upon charge/discharge cycling in aqueous electrolytes. Possible degradation mechanisms, including material dissolution, are discussed. To test these possible mechanisms, an agar gel coating is deposited on the films to reduce mass transport between the electrode/electrolyte interface. The electrochemical cycling behavior of vanadium oxide films with various surface treatments is investigated at different pH. Quantitative compositional analysis and morphological studies provide additional insight into the mechanism responsible for capacitive degradation.

1. Introduction

In 2011 the world's population exceeded 7 billion. Energy demand is at an all time high, and it will only go up. An essential part of this energy demand is its capture, storage and release, and although traditional batteries and capacitors have dominated this area, electrochemical capacitors have emerged as a complementary technology with unique energy storage characteristics.

Generally referred to as electrochemical capacitors, these devices include supercapacitors and ultracapacitors, which were coined by Nippon Electric Company and Pinnacle Research Institute, respectively. These electrical energy storage devices bridge the gap between high power density capacitors and high energy density batteries [1]. These devices are utilized in high pulsed-power and time-dependent usage applications, such as power sources in hybrid electric vehicles and as backup sources for memories and microcomputers [2]. Much broader deployment is

* Corresponding author. Tel.: +1 510 642 5771; fax: +1 510 642 9178.
E-mail addresses: allison.engstrom@berkeley.edu (A.M. Engstrom), fmdoyle@berkeley.edu (F.M. Doyle).

0378-7753/$ – see front matter © 2012 Elsevier B.V. All rights reserved.
http://dx.doi.org/10.1016/j.jpowsour.2012.11.075

clearly possible when one considers the potential for capturing and redirecting large bursts of waste energy over short timespans to improve energy efficiency.

The two types of electrochemical capacitors are characterized by their primary charge storage mechanisms: those that store energy in the electrochemical double layer and those that also exhibit pseudocapacitance. Electrical double layer capacitors store energy by charge separation across the double layer that exists between the electrode surface and the electrolyte. High surface area materials, such as activated carbon, are commonly used for this technology. In addition to double layer charging, materials that exhibit pseudocapacitance store charge via reversible Faradaic reduction or oxidation (redox) reactions. For transition metal oxides, the redox reactions may simply be reduction and oxidation between the transition metal oxidation states. As the redox reactions take place in the material, local charge-buildup is compensated by intercalation of ions from the electrolyte [3]. Fig. 1 illustrates this mechanism for a whole cell electrochemical capacitor device. Upon charging, the cathode undergoes reduction, which induces the cations from the electrolyte to intercalate into the structure. Meanwhile, oxidation occurs at the anode, where the cations deintercalate.

For the vanadium oxide system, Equation (1) shows the equilibrium between V(V) oxide, monovalent cations from the electrolyte, M^+, and the oxide in which the V(V) has been reduced to V(IV) (without disruption of the oxide lattice), with the resulting charge compensated by intercalation of the monovalent cations. The position of equilibrium is clearly dependent upon the electrochemical potential; thus, the potential can be manipulated to control the direction of current flow.

$$(V_2O_5)_{surface} + 2M^+ + 2e^- \leftrightarrow \left(V_2O_5^{2-}M_2^{2+}\right)_{surface} \quad (1)$$

The metal oxides most widely studied for electrochemical capacitor applications are RuO_2 and MnO_2. Unfortunately, RuO_2 is expensive and toxic, while MnO_2 can only be used at high-pH in aqueous environments. Vanadium oxide is only five percent the cost of RuO_2, and it has been shown to discharge 1.6 times faster [4]. Although nanostructured vanadium oxides may be synthesized in a variety of methods, electrochemical deposition provides a means of controlling the surface morphology and crystallinity by varying the electrochemical parameters [5–16].

Despite the attractive initial capacitance, vanadium oxide films typically exhibit performance degradation during cycling, particularly in aqueous environments, which are intrinsically attractive because of their high conductivity; material dissolution may be the primary cause [17]. In the current work, vanadium oxide films were synthesized by anodic electrodeposition, and an agar gel coating was tested as a means of reducing mass transport of dissolved vanadium species from the surface of the electrode in aqueous media. These structures were used to investigate not only the V_2O_5, but also the V_2O_4 and V_2O_3 aqueous stability regimes. The capacitive and cycling performance of the oxide and oxide/gel electrodes were tested in various aqueous environments.

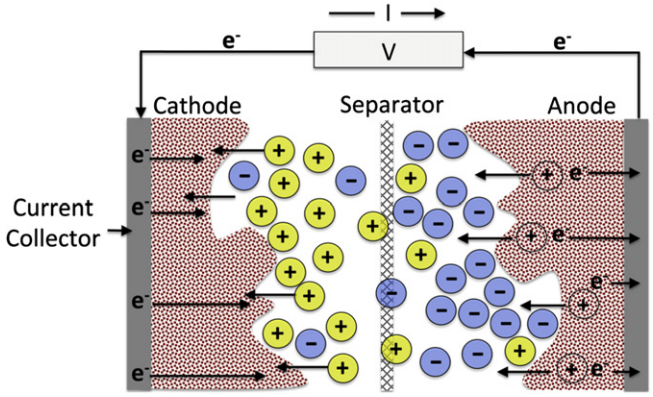

Fig. 1. Charging of an electrochemical capacitor device containing transition metal oxide anode and cathode materials. The metal oxidation state is reduced at the cathode, which induces cations to intercalate from the electrolyte. In contrast, oxidation at the anode causes deintercalation.

2. Experimental methods

2.1. Electrochemical synthesis

Vanadium oxide films were synthesized using a three-electrode cell comprising a saturated KCl Ag/AgCl reference electrode (0.199 V vs. SHE) from Koslow Scientific, a 5 × 5 cm Pt gauze from Sigma Aldrich as the counter electrode and a 0.5 cm diameter planar Pt electrode for the working electrode and substrate for the vanadium oxide. The films were deposited at 1.1 V vs. Ag/AgCl in 1.0 M $VOSO_4$, 0.1 M Na_2SO_4, pH 1.8 aqueous solution prepared using 18 MΩ Millipore water. A total of 3.0 C of charge was passed. The pH was selected to correspond to the solubility minimum for V_2O_5 under oxidizing conditions [18]. The potentiostatic deposition potential was chosen at the center of the broad deposition peak on an anodic 2 mV s^{-1} linear voltammetric sweep from the open circuit potential until the initiation of oxygen evolution. Following deposition, the films were rinsed in water, 18 MΩ Millipore, and dried either under N_2 flow at 25 °C for approximately 5 min or in a dry oven at 100 ± 10 °C for 30 min, then at 25 °C for an additional 5 min. The vanadium oxide films weighed 0.3 ± 0.1 mg (measured for several samples).

2.2. Electrochemical characterization

The oxides were electrochemically characterized in 1.0 M aqueous KCl at pH 1.8, 3.0, 5.0 or 7.5 using cyclic voltammetry (CV) and galvanostatic charge/discharge (CD) cycles between potential ranges of −0.15 to 0.85, −0.25 to 0.75, −0.35 to 0.65 or −0.55 to 0.45 V vs. Ag/AgCl, respectively. Arrows in the E–pH diagram shown in Fig. 2 depict these ranges. The diagram is plotted for three different activities, a, of dissolved species, namely 0.01, 1, and 100 (the thickness of the lines separating predominance regions increases with an increase in activity). Although the higher activities are unrealistic for bulk solutions, high concentrations and activity coefficients are not inconceivable in the boundary layers adjacent to electrodes during dissolution.

The specific capacitance was calculated from the CV and galvanostatic CD curves (see Fig. 3a and b for examples) using Equations (2) and (3), respectively, where i is the galvanostatic current, t_{disch} is the time spent during the discharge portion of the cycle, V_{window} is the potential window, m is the mass of the deposited vanadium oxide film and ν is the CV scan rate.

$$C_{S,CV} = \left(\int_{disch} i dV\right) \Big/ (V_{window} \nu\, m) \quad (2)$$

$$C_{S,CD} = (i\, t_{disch})/(V_{window}\, m) \quad (3)$$

The electrolyte pH was measured with an Orion, Thermo Scientific 915600 pH electrode connected to an Orion 290A pH meter calibrated with pH 7.0, 4.0 and 1.0 buffer solutions prior to each measurement. The pH of each aqueous KCl solution was

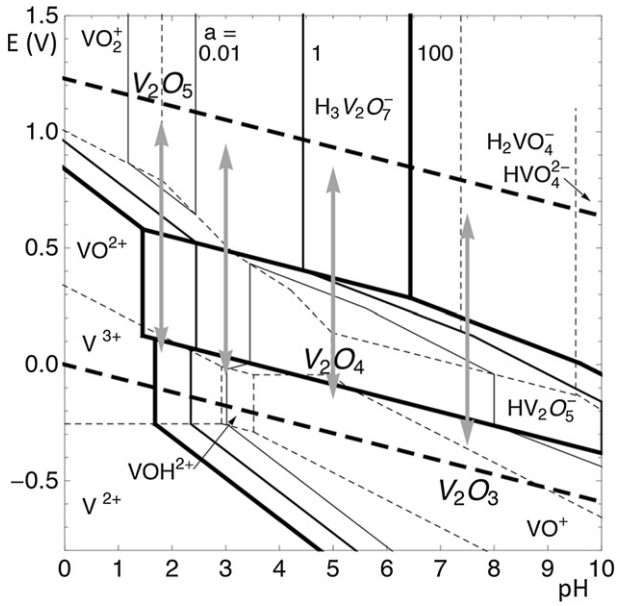

Fig. 2. E–pH diagram of the vanadium–water system for various activities of the dissolved species plotted at $a = 0.01, 1$ and 100. Solid lines indicate equilibria involving at least one solid species whereas the dashed lines separate the predominance regions of two dissolved species. The arrows depict the potential ranges (SHE) and pH's at which the vanadium oxide films were tested. Thermodynamic data were taken from Ref. [18].

adjusted using HCl and KOH. Electrochemical deposition as well as CV and galvanostatic CD measurements were performed using a PAR 273 potentiostat.

Electrochemical Impedance Spectroscopy (EIS) was performed using a Gamry Series G™ potentiostat and modeled using Echem Analyst™ Software. The impedance of the vanadium oxide films with and without an agar gel coating was measured in 1.0 M aqueous KCl at pH 3.0. The AC voltage amplitude was set to 10 mV with respect to the open circuit potential vs. Ag/AgCl over a frequency range of 100 kHz–10 mHz.

2.3. Gel synthesis and deposition

Gel coatings with an agar concentration of 6.67 g L^{-1} were prepared by dissolving agar powder in either boiling water [19] or 1.0 M KCl at pH 6. Ideally the aqueous phase within the agar gel would be identical to the test electrolyte. After preliminary work had identified pH 3.0 as the most promising pH, gel coatings were also prepared with 1.0 M pH 3.0 KCl. However, because gelation of agar is pH-dependent (gelation involves the formation of helices stabilized by the hydroxyl groups through hydrogen bonding [20], which is disrupted by protonation of the hydroxyl groups at low pH), gels made with 6.67 g L^{-1} agar concentration in pH 3.0 electrolyte were mechanically weak. Therefore some of the pH 3.0 gels utilized 13.34 g L^{-1} agar. Agar solutions were cooled to 50 °C under forced convection for approximately 30 min, by which time visual inspection indicated that gelation had commenced, with concurrent increase in viscosity. The desired volume was drop-deposited on the dry vanadium oxide film. Upon complete gelation, the electrode was transferred to the testing electrolyte.

2.4. Compositional and morphological characterization

In order to characterize the vanadium materials, they were prepared electrochemically, as described above, but using a modified working electrode that could be removed for *ex situ* examination without disrupting the deposited films. A 7.0 mm square Pt foil was placed over the 0.5 cm diameter planar Pt electrode, which provided electrical connection. A mask made by punching a 0.5 cm diameter hole in a Parafilm® M sheet was placed over the foil to secure it to the Pt electrode while exposing the same surface area as in the previous electrodeposition experiments. After deposition and cycling the Parafilm® M was removed, leaving the vanadium

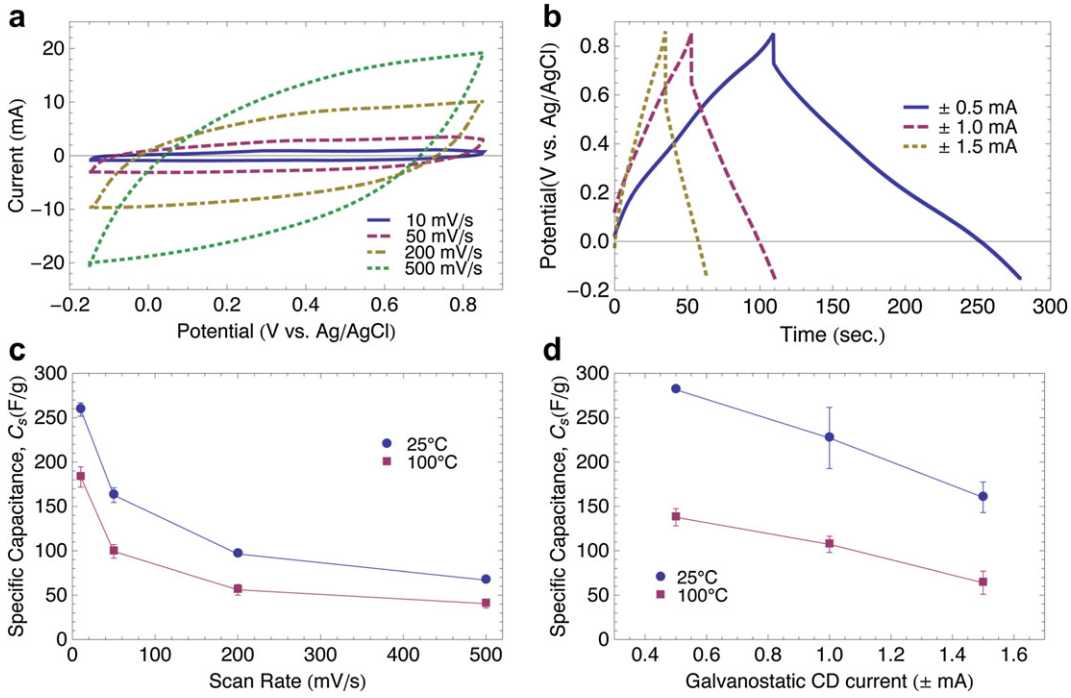

Fig. 3. As-deposited vanadium oxide films dried at 25 °C and tested in 1.0 M KCl at pH 1.8 using a) cyclic voltammetry (CV) and b) galvanostatic charge/discharge (CD) cycles at various scan rates and currents, respectively. The specific capacitance was then calculated from the c) CV and d) galvanostatic CD cycles using Equations (2) and (3), respectively, for both the 25 °C N_2 flow and 100 °C dry oven drying procedures.

oxide on the Pt foil substrate. The vanadium oxide films were synthesized by anodic potentiostatic electrochemical deposition in 1.0 M $VOSO_4$, 0.1 M Na_2SO_4 at pH 1.8 aqueous solution using 18 MΩ Millipore water at 1.4 V vs. Ag/AgCl until 3.0 C of charge had passed. The potentiostatic deposition potential for the Pt foil electrodes was chosen using the same procedure as the planar Pt electrode as described in Section 2.1. Although the electrodes exhibited slightly different polarization behavior, the chosen potential in both cases ensured transport-controlled deposition. After deposition, the films were rinsed in water, 18 MΩ Millipore, and dried under N_2 flow at 25 °C. Agar was prepared and deposited as described in Section 2.3. The cycled electrodes were prepared by performing thirty (30) ± 0.5 mA galvanostatic CD cycles in 1.0 M aqueous KCl at either pH 1.8, 3.0, 5.0 or 7.5 between potential ranges of −0.15 and 0.85, −0.25 and 0.75, −0.35 and 0.65 or −0.55 and 0.45 V vs. Ag/AgCl, respectively. The agar coating was removed by briefly contacting with the testing electrolyte at an elevated temperature, approximately 100 °C. All electrodes were then dried under N_2 flow at 25 °C and stored under Ar until further analysis.

Quantitative compositional analysis of the films, on the Pt foil substrates, was performed using a Cameca SX-51 electron microprobe for wavelength dispersive spectrometry (WDS). The morphology of the as-deposited and cycled films was examined with a Leo 430 SEM.

3. Results and discussion

3.1. Pseudocapacitive behavior of as-deposited vanadium oxide

Electrodeposited vanadium oxide films dried at 25 °C under N_2 flow exhibit pseudocapacitive behavior when subsequently cycled using either CV or galvanostatic CD methods in 1.0 M aqueous KCl at pH 1.8, as shown in Fig. 3a and b. The large CV hysteresis and lack of defined peaks indicate that the total capacitive behavior is due not only to double layer charging, but also to reversible redox reactions involving a nearly continuous electron transfer mechanism [3]. This suggests that a pseudocapacitive mechanism such as described in Equation (1) could be at work. The film dried at 100 °C in the dry oven exhibited the same basic shape but with lower current density (CV) or faster discharge times (CD).

The specific capacitance for samples prepared by both drying procedures was calculated from the CV and galvanostatic CD data using Equations (2) and (3), and is plotted in Fig. 3c and d, respectively. The decrease in capacitance with increasing scan rate would be expected for highly porous materials such as these because the ion intercalation and deintercalation process depends upon mass transfer from the electrolyte through the porous network. Under fast charge/discharge conditions this limits the accessibility of the charge storage potential of the bulk material.

As the CV scan rate or galvanostatic CD current is increased, the time required for each cycle decreased. The decrease in capacitance with increasing scan rate or current raises the possibility that the reduced cycle time, rather than the scan rate *per se*, limits the charge stored by pseudocapacitance. The limiting factor may be electrical transport due to the poor electrical conductivity of the oxide, or mass transport associated with intercalation throughout the porous network. For either CV or galvanostatic CD testing, the film dried at 25 °C with N_2 exhibited a larger pseudocapacitive response than the film dried at 100 °C. This is probably due to a reduction in surface area upon coarsening at the higher temperature. It is also possible that dehydration inhibits wetting of the oxide surface when returned to the electrolyte, making part of the surface inaccessible.

The cycle lives of the as-deposited oxide films were investigated by 500 mV s^{-1} CV and ±0.5 mA galvanostatic CD analysis as plotted in Fig. 4a and b, respectively. The specific capacitance, calculated from each of these cycles using Equations (2) and (3), is plotted in Fig. 4c and d. Whether cycled under CV or galvanostatic CD, the capacitance of the oxides decreased with protracted cycling, albeit

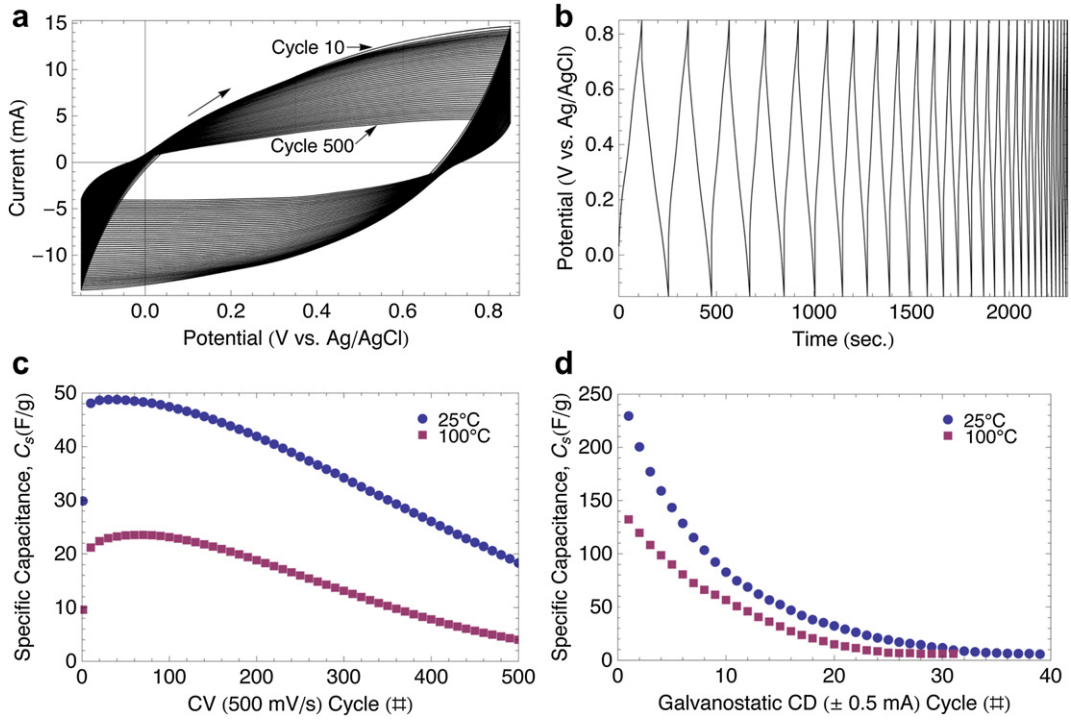

Fig. 4. Cycle behavior of the as-deposited vanadium oxide dried at 25 °C and tested in 1.0 M KCl at pH 1.8 using a) CV at 500 mV s^{-1} and b) galvanostatic CD with ±0.5 mA. The cycle lives for both the 25 °C and the 100 °C drying procedures are compared for the c) CV and d) galvanostatic CD cycling.

after an initial increase in the case of CV cycling. The drying procedure did not significantly affect the rate of degradation, but since the 25 °C drying procedure gave higher capacitances, all following investigations utilized oxide dried at 25 °C.

It is striking that the capacitance decreased much faster under galvanostatic CD cycling than under CV conditions, but that the initial capacitance values were much higher for galvanostatic CD cycling than for CV cycling. A major difference between these two cycling techniques is the time required for a total charge/discharge cycle. Fig. 3b shows that it took about 280 s for the ±0.5 mA galvanostatic CD current to complete a cycle, whereas when scanning at 500 mV s^{-1} the CV scan only took 4 s, almost two orders of magnitude faster. The slower charging under galvanostatic conditions at low current would be expected to yield higher capacitance, given the relatively slow kinetics that would be expected for intercalation. Less obviously, however, the differences in charging/discharging rates could also account for the differences in degradation rate if the degradation mechanism was mass transport limited. Visual inspection revealed that after cycling, the oxide film coverage on the underlying platinum substrate and its volume were diminished, suggesting partial dissolution of the oxide into the electrolyte. From Fig. 2, it is evident that at pH 1.8 V_2O_5 is the predominant species at the higher potentials reached during cycling; however, this will be in equilibrium with low activities of VO_2^+ (Equation (4)) and undergoes reductive dissolution to VO^{2+} at the lower potentials (Equation (5)) [18].

$$(V_2O_5)_{surface} + 2H^+ \leftrightarrow 2VO_2^+ + H_2O \quad (4)$$

$$\left(V_2O_5^{2-}\right)_{surface} + 6H^+ + 2e^- \leftrightarrow 2VO_2^{2+} + 3H_2O \quad (5)$$

Consequently, reductive dissolution would be most pronounced during the cathodic discharge curve when the potential is approaching the lower bound. Therefore, it is instructive to compare the amount of charge passed during the charging and discharging curves of each cycle; differences in these values would suggest irreversible processes. Fig. 5 reports the ratio of the charge passed during the cathodic discharge half-cycle to the charge passed during the anodic charging half-cycle. A value of 1 is ideal for electrochemical capacitor systems, and a value greater than 1 implies that not all of the charge passed during discharge can be returned to the oxide during charging. The most likely explanation is that some of the charge is passing as reductive dissolution, rather than solid-state reduction with compensating intercalation, followed by transport of the dissolved V species away from the electrode, so that they are not available for redeposition during the charging half-cycle. The deviation from ideal behavior is much more pronounced for the galvanostatic CD scan, and it appears to increase until cycle 35, at which point the capacitance has declined to zero (Fig. 4d), and the material has failed. Given the longer cycle times of the galvanostatic CD conditions, this is consistent with some reductive dissolution. In contrast, during the relatively short CV cycles, less time is available for dissolution and subsequent mass transfer away from the electrode surface, so one would expect less degradation, and hence behavior closer to ideality, in a given cycle.

Although the observed behavior is consistent with reductive dissolution, capacitive degradation may also be due to reduction of the surface area upon cycling, due to smoothing induced by surface diffusion or dissolution/reprecipitation. Smoothing could also be affected by the magnitude of the current passed per cycle. The maximum current passed during the CV cycles was approximately forty (40) times greater than the maximum current tested under galvanostatic CD conditions. Lower current densities are known to promote smoother, more crystalline structures while higher current densities promote higher surface area nodular or dendritic structures [21]. A reduction in surface area over many cycles would certainly reduce the measured capacitance by limiting the mass transport of intercalation ions to the bulk of the oxide.

3.2. Vanadium oxide films using agar gel coating

To further study the degradation of the oxide films, agar gel coatings were applied to reduce the mass transport between the electrode surface and the bulk electrolyte. Agar was selected for the gel barrier because it gels below 50 °C and it is easily dissolved at elevated temperatures. Initially, it was necessary to investigate how the gel would affect the as-deposited vanadium oxide. As shown in Fig. 6, the pseudocapacitive properties were greatly diminished for agar prepared using only water, particularly for the thickest gel layers. This could indicate that the gel hindered the transport of cations from the testing electrolyte to the surface, thereby reducing ion intercalation, or it could be due to the higher resistivity of the gel. Agar gel prepared using 1.0 M aqueous KCl at pH 6.0 applied over vanadium oxide yielded pseudocapacitive properties strikingly similar to those of V_2O_5 alone. The KCl in the agar gel provides surface proximity for ionic intercalation species and improves the conductivity of the gel.

It is, of course, possible that agar itself contributed to the measured capacitance. Fig. 7 shows cyclic voltammograms

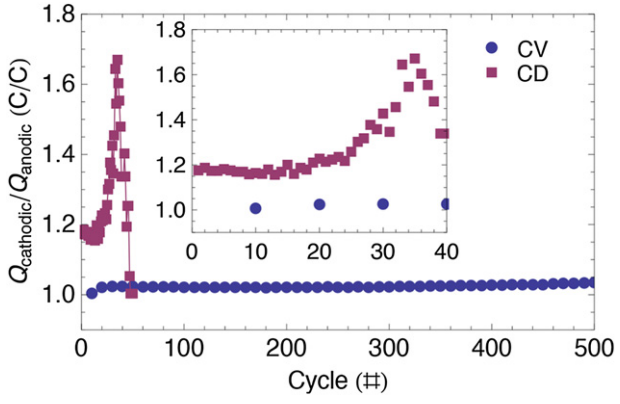

Fig. 5. Comparison of the ratio of the charge passed during the cathodic discharge half-cycle to the charge passed during the anodic charging half-cycle with cycle life using 500 mV s^{-1} CV and ±0.5 mA galvanostatic CD on as-deposited vanadium oxide film dried at 25 °C.

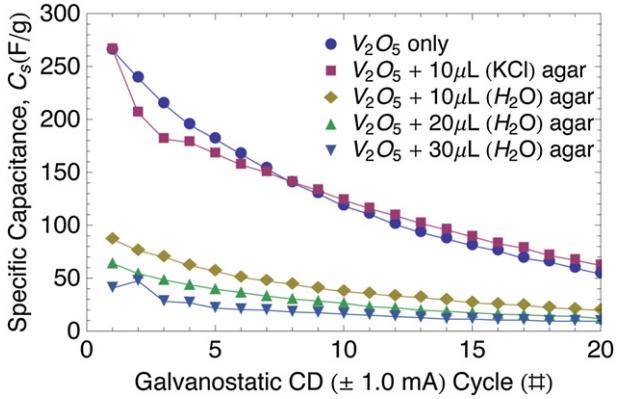

Fig. 6. Pseudocapacitive behavior of vanadium oxide as-deposited and with various amounts of agar gel prepared with 6.67 g L^{-1} agar in either water or 1.0 M KCl and tested with ±1.0 mA galvanostatic CD in 1.0 M KCl at pH 1.8.

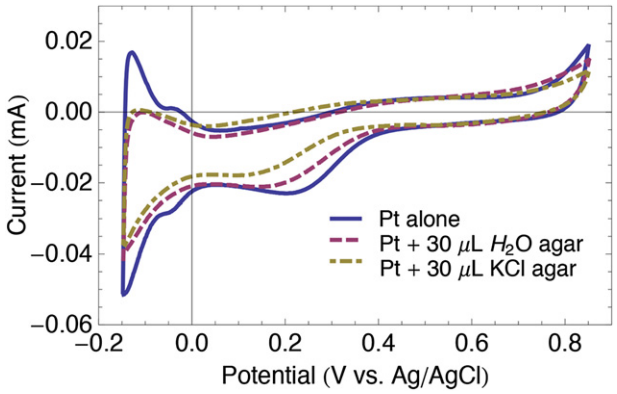

Fig. 7. Cyclic voltammetry at 50 mV s^{-1} of the Pt alone and with a gel prepared with 6.67 g L^{-1} agar powder in water or 1.0 M KCl.

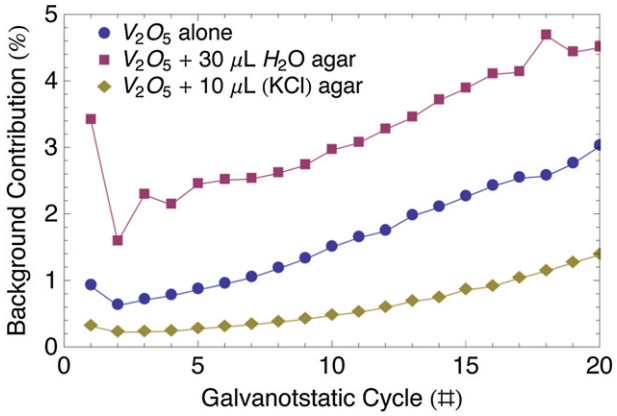

Fig. 8. Background contribution for galvanostatic cycles of the Pt alone and with a gel prepared with 6.67 g L^{-1} agar powder in water or 1.0 M KCl.

obtained at 50 mV s^{-1} in 1.0 M KCl at pH 1.8 for a clean Pt surface, a 30 μL drop of agar prepared with water and a 30 μL drop of agar prepared with 1.0 M KCl on a clean Pt surface. The agar gel seems to block the Pt surface from H adsorption and Pt oxidation, as indicated by the reduced redox peaks. These peaks are non-capacitive in nature, and thus are ignored when discussing any contribution to the capacitance of the system. When compared to cyclic voltammetry of the oxide alone and the oxide/agar gel electrodes, the agar or Pt potentially contributes less than 2% to the measured capacitance.

Considering the background contribution to the galvanostatic cycle data, Fig. 8 plots this percentage over several galvanostatic CD cycles. The contribution was calculated by performing galvanostatic cycling for the Pt alone as well as Pt with water or KCl based agar then normalizing the capacitance response to the data from the electrodes containing vanadium oxide. The background contribution increases with increasing cycles because the capacitance response from the vanadium oxide decreased. For cyclic voltammetry and galvanostatic cycle measurements, the Pt substrate and agar coating seem to have a relatively insignificant contribution to the overall capacitance.

3.3. Vanadium oxide/gel cycle life in various V_xO_y stability regimes

It is apparent from Fig. 6 that even with agar gel inhibiting mass transport, the capacitance of the vanadium oxide films still declined with cycling. In these systems, the agar gel was a modest 10 μL volume dropped over a 0.196 cm^2 planar surface area, providing a very short distance from the electrode surface to the electrolyte. For comparison, Fig. 9, shows the effect of cycling on V_2O_5 alone and V_2O_5 with the maximum amount of agar gel that could be dropped on the electrode surface, approximately 400 μL.

These systems were tested in 1.0 M KCl at pH 1.8, 5.0 and 7.5 which, as mentioned above, correspond to the V_2O_5, V_2O_4 and V_2O_3 stability region; however, these electrodes were also studied at pH

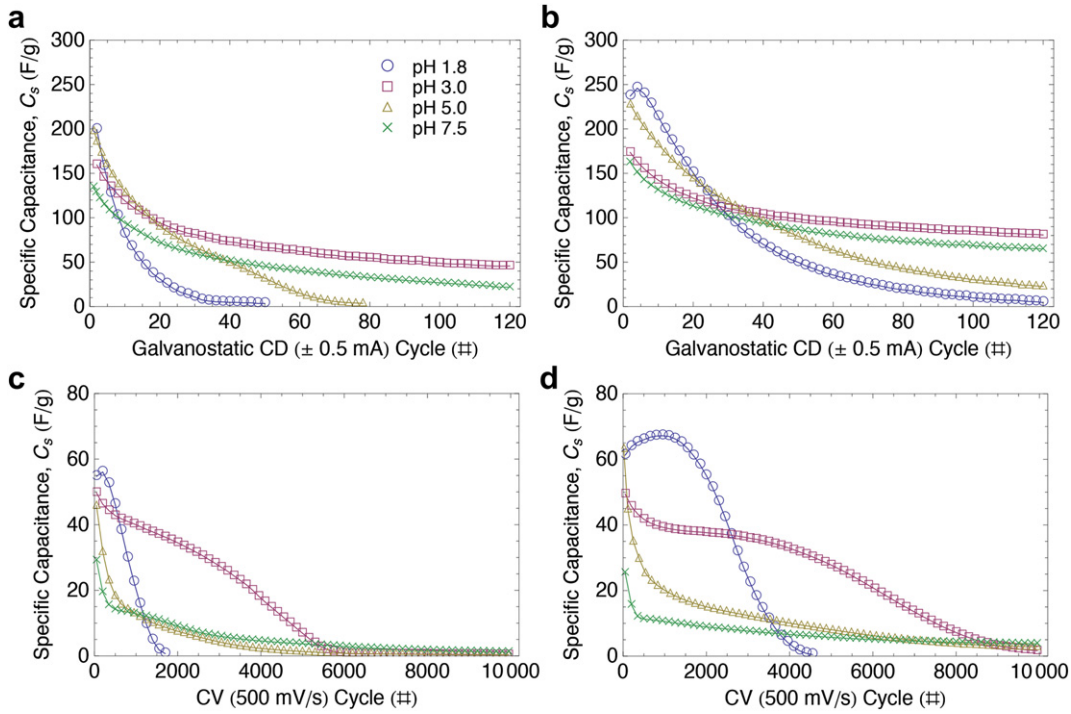

Fig. 9. Cycle behavior of vanadium oxide using ±0.5 mA galvanostatic CD on a) V_2O_5 alone and b) V_2O_5 with approx. 400 μL KCl agar gel and tested using 500 mV s^{-1} cyclic voltammetry on c) V_2O_5 alone and d) V_2O_5 with approx. 400 μL KCl agar gel.

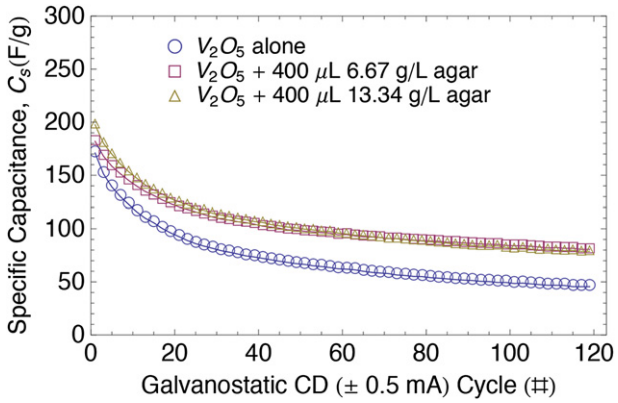

Fig. 10. Cycle behavior of vanadium oxide using ±0.5 mA galvanostatic CD on V_2O_5 alone and V_2O_5 with approximately 400 μL agar gel prepared with either 6.67 or 13.34 g L^{-1} agar powder in 1.0 M pH 3.0 KCl.

3.0, which is an intermediate region that corresponds to the maximum stability region for all three solid oxide forms (see Fig. 2), using a higher agar concentration to ensure gelation. Fig. 10 demonstrates that the higher agar concentration did not alter the initial capacitance or cycle behavior.

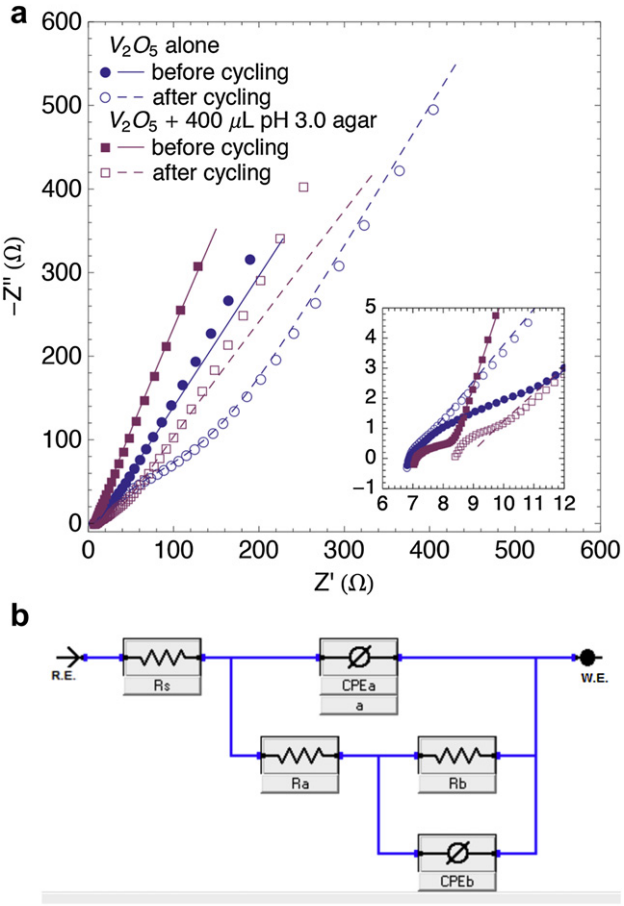

Fig. 11. EIS (a) Nyquist plot and (b) equivalent circuit model for vanadium oxide with and without 400 μL agar gel prepared with 13.34 g L^{-1} agar powder in 1.0 M pH 3.0 KCl. EIS was performed before and after thirty (30) ± 0.5 mA galvanostatic CD cycles in 1.0 M pH 3.0 KCl. The markers represent the data, and the lines represent the fitted model using the parameters reported in Table 1.

Table 1
EIS fitting parameter results.

Parameter	Units	V_2O_5 alone		V_2O_5 + 400 μ L^{-1} pH 3.0 agar	
		Before cycling	After cycling	Before cycling	After cycling
R_a	ohms	6.2	286.5	1.5	55.2
R_s	ohms	6.9	6.9	7.1	8.8
A (CPE_a)	mS s^a	2.76	3.63	5.89	4.76
a		0.6152	0.5725	0.6226	0.5127
B (CPE_b)	mS s^b	14.0	7.51	20.7	7.00
b		0.6436	0.7193	0.8254	0.6847
R_b	Gohms	0.6	371.3	10.4	684.7
Goodness of fit		3.86E-04	5.00E-04	1.26E-04	1.60E-03

For both the ±0.5 mA galvanostatic CD and 500 mV s^{-1} CV cycle data, the agar-coated electrodes exhibited an improved cycle life over the oxide alone. The larger volume and thus increased distance from the surface to the electrolyte seems to impede mass transport. Also, for all systems, the cycle life is drastically higher for the CV testing than for the galvanostatic CD tests. As discussed above, this is most likely due to dissolution-related material loss attributed to longer galvanostatic CD cycle times or to surface area reduction from smoothing by the lower currents applied in galvanostatic CD cycling.

Examination of the behavior at different pH uncovers trends that exist independent of whether agar coats the oxide surface. The initial capacitance response is largest at pH 1.8; however, the cycle life is inferior to that at higher pH. The small increase in capacitance near the beginning of testing may be due to a surface area increase during the high current CV scans. The initial capacitance was

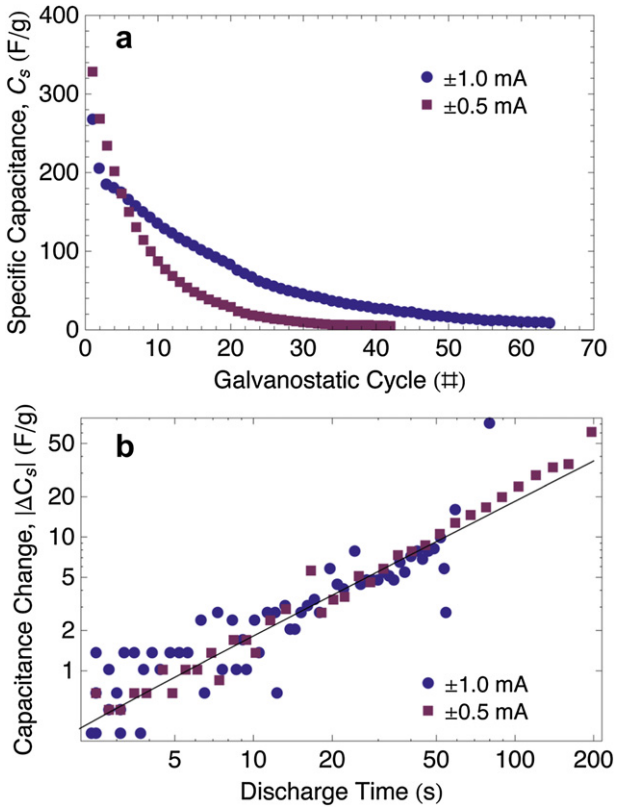

Fig. 12. Vanadium oxide with a 10 μL 1.0 M pH 6.0 KCl agar coating cycled using galvanostatic CD cycles at ±0.5 and ±1.0 mA. This figure reports the same data where a) shows the capacitance behavior over many cycles and b) shows the change in capacitance as a function of the total time passed during discharge.

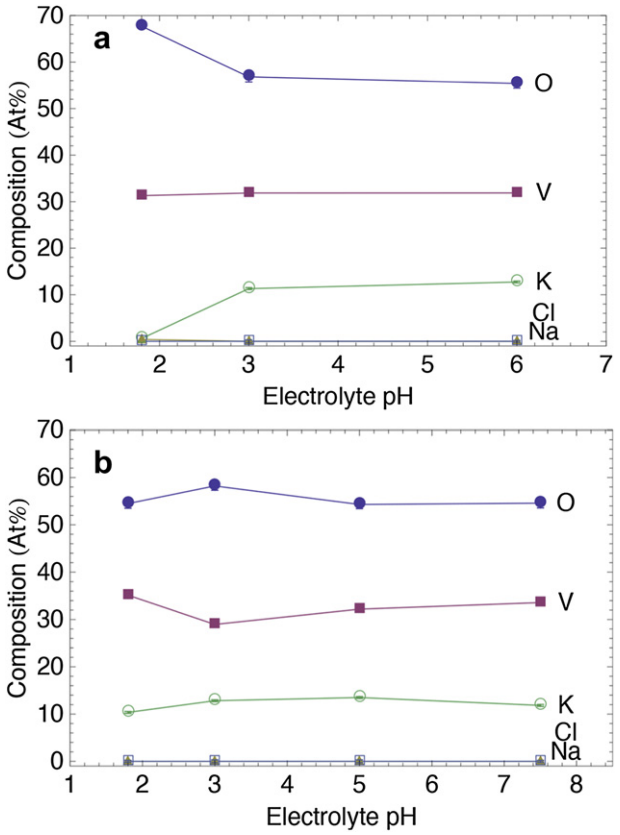

Fig. 13. Sample composition of the a) as-prepared and b) cycled vanadium oxide electrodes exposed to various pH environments measured by WDS. The amount of stoichiometric K^+ and Cl^- representing excess electrolyte on the surface was subtracted from the data.

slightly lower at pH 5.0, but the capacitance was retained better over its cycle life. At pH 7.5 the initial capacitance was even lower, but the capacitance retention was better than at pH 5.0. The most promising environment was at pH 3.0; despite its moderate initial capacitance, its superior capacitance retention provided a longer cycle life for both the CV and galvanostatic CD testing. Since the pH 3.0 environment represents the minimal solubility region, the fact that it exhibits the longest cycle life supports the hypothesis that degradation is dominated by dissolution.

To further explore the electrochemical behavior of the vanadium oxide half-cells, EIS was performed on the three-electrode systems

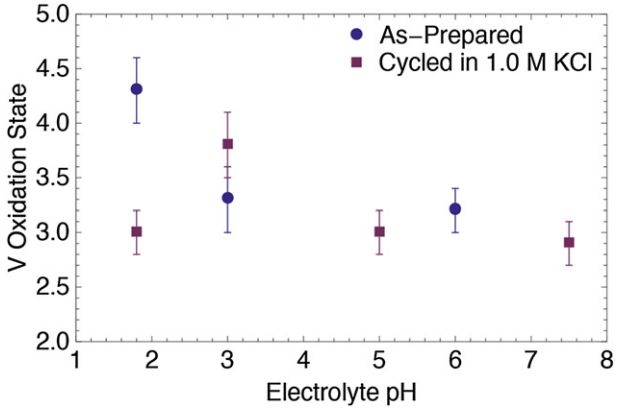

Fig. 14. Average vanadium oxidation state of the as-prepared and cycled electrodes calculated from WDS data of the samples exposed to various aqueous environments.

with and without the agar gel coating as well as before and after thirty (30) ± 0.5 mA galvanostatic CD cycles. The Nyquist plot is reported in Fig. 11a, and the equivalent circuit model used to fit the data is illustrated in Fig. 11b. The model utilizes constant phase elements (CPEs) rather than capacitive elements to account for the non-ideal behavior of capacitors during EIS. The impedance of the CPEs is described in Equation (6) where ω is the frequency and j is $\sqrt{-1}$. The equation describes the behavior of ideal capacitor elements when the exponents a and b are equal to 1.

$$Z_{\mathrm{CPE}_a} = 1/[A\cdot(j\omega)^a]$$
$$Z_{\mathrm{CPE}_b} = 1/[B\cdot(j\omega)^b] \quad (6)$$

The resistive parameters, R_S and R_a, represent the equivalent series resistance (ESR) and the charge-transfer resistance, respectively. The constant phase element, CPE_a, is related to the double layer capacitance, and the parallel elements, R_b and CPE_b, have replaced the typical Warburg impedance and pseudocapacitive elements that represent the passage of DC across the electrode/electrolyte interface [22].

The fitting parameter results are listed in Table 1. Comparing the two oxide surface preparations before cycling, the ESR is not significantly different, but the R_a is smaller for the sample containing the agar gel coating. Also, the CPE_a and CPE_b values are larger for the sample with the gel coating, which is consistent with capacitive data in Fig. 10 where the samples containing agar had a larger initial capacitance as compared to the oxide alone. Comparing the samples before and after cycling, the resistive elements, R_a and R_b, increase significantly with cycling, and the CPE_b decreases. This result is consistent with the observed capacitive degradation with cycling in Fig. 10. Lastly, it is observed that the ESR remains constant during cycling for the oxide without agar; however, the sample with the agar coating exhibits a relatively small increase in ESR after cycling. One possible explanation for this behavior is the accumulation of dissolved species in the agar gel near the oxide surface due to a reduction in mass transport. The presence of the bulky dissolved ionic species in the solution of the gel matrix would likely reduce the electrolyte conductivity. The EIS results appear to be consistent with the cycle behavior observed for the galvanostatic CD data, and they offer additional support that dissolution occurs upon cycling.

Further electrochemical support for the dissolution-related degradation hypothesis is provided by Fig. 12, which relates the degradation rate to the length of discharge for galvanostatic CD experiments using 10 μL 1.0 M KCl agar at pH 6.0 cycled at ±0.5 and ±1.0 mA. Whereas Fig. 12a appears to show two distinctly different curves, Fig. 12b replots the same data to show the change in capacitance as a function of the time spent during the discharge portion of the cycle. Although the cycle lives differ for the two galvanostatic current conditions, the change in the capacitance seems to depend linearly on the length of time of discharge and be independent of the current itself. A longer cycle time (lower current) would allow for more dissolution and thus more degradation. Thus the behavior depicted in Fig. 12 further supports the hypothesis that dissolution is responsible for degradation.

3.4. Quantitative compositional analysis with WDS

Compositional analysis of the oxides was performed using WDS. Fig. 13 shows the composition as a function of the electrolyte pH environment for both the as-prepared and cycled samples. The vanadium oxide was deposited at pH 1.8 and rinsed in water. No Na was detected by WDS, indicating that rinsing was effective. The data points at higher pH values for the as-prepared samples in

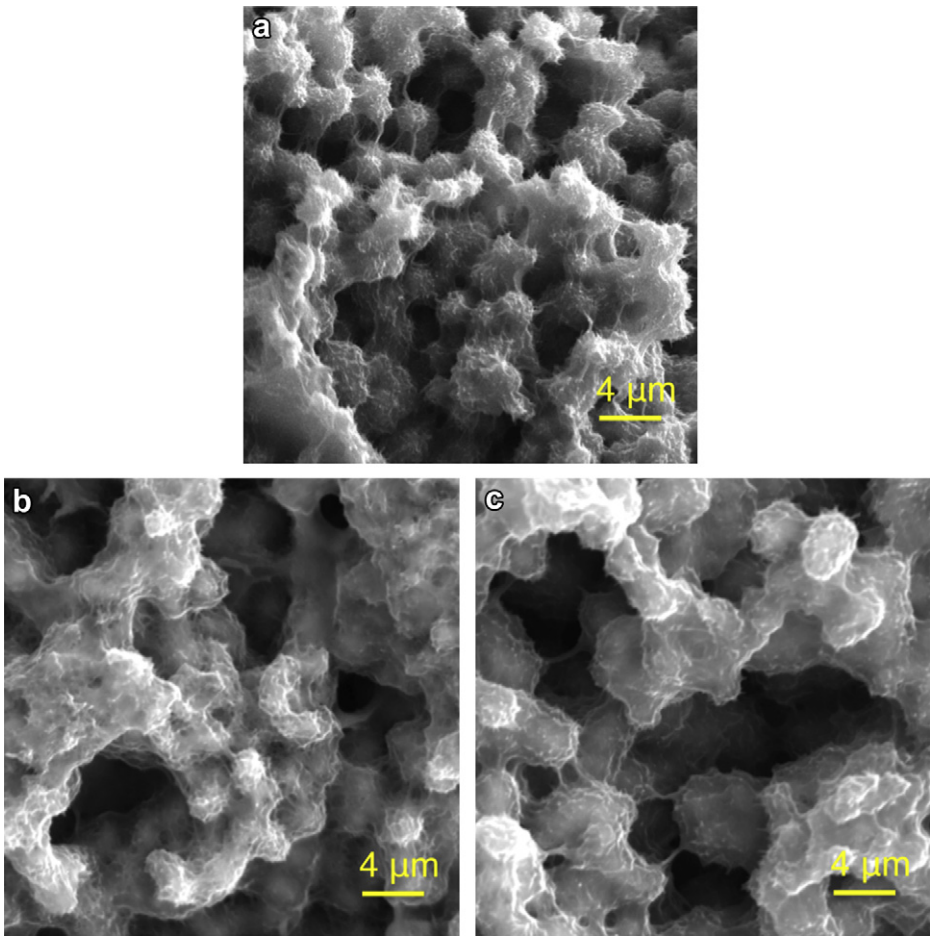

Fig. 15. Secondary electron images of as-prepared a) vanadium oxide alone, b) vanadium oxide coated with 1.0 M, pH 3.0 KCl agar that was removed before SEM analysis and c) vanadium oxide coated with 1.0 M pH 6.0 KCl agar that was removed before SEM analysis. Agar coatings were removed using electrolyte at approximately 100 °C.

Fig. 13a represent oxide films that had been deposited and subsequently coated with an agar film containing an aqueous phase at either pH 3.0 or pH 6.0. The agar was then removed by briefly contacting with the testing electrolyte at an elevated temperature, approximately 100 °C. The cycled samples underwent galvanostatic CD cycling after coating with agar, which was removed post-cycling. The samples that had had an agar coating applied and removed were not rinsed with water, as the resulting change in pH may have induced compositional changes. Although as much solution as possible was removed before drying the oxides, K^+ and Cl^- are present in all samples that had been coated with gel. The amount of stoichiometric K^+ and Cl^- representing this excess electrolyte was subtracted from the raw data and is not reported in Fig. 13. For all samples that had been coated with gel, an excess of K^+ was detected in the oxide films, presumably due to intercalation into the oxide. According to the mechanism for pseudocapacitance, K^+ intercalation occurs during the reduction half-cycle to compensate for the negative charge build-up. Therefore, an excess amount of K in the oxide indicates an overall reduction in the vanadium oxidation state.

To examine the data further, the WDS data reported in Fig. 13 were used to determine the vanadium oxidation state for the various stages of testing. The empirical formula for the vanadium oxide detected by WDS is represented by $N(V_2^{x+}O_x^{2-})$ where $x+$ is the average oxidation state of the vanadium, and the value N is a weighting factor. The stoichiometric relationship between the ionic abundance and oxidation state led to the definitions in Equation (7) where $[X]$ is the WDS-measured concentration of X and $[O]_{Kint}$ is the concentration of oxygen whose negative charge is compensated by intercalated potassium ions, namely by the stoichiometric excess of K^+.

$$\begin{aligned} xN &= \left[O^{2-}\right] - \left[O^{2-}\right]_{Kint} \\ 2N &= \left[V^{x+}\right] \\ \left[O^{2-}\right]_{Kint} &= 1/2K^+_{excess} = 1/2\left(\left[K^+\right] - \left[Cl^-\right]\right) \end{aligned} \tag{7}$$

Solving for x from Equation (7) led to Equation (8) where the WDS data were used to calculate the average vanadium oxidation state.

$$x+ = \left(2\left[O^{2-}\right] - \left[K^+\right] + \left[Cl^-\right]\right) \Big/ \left[V^{x+}\right] \tag{8}$$

The calculated vanadium oxidation state for the as-prepared and cycled samples is reported as a function of pH in Fig. 14. The as-deposited oxide, which did not contain a gel coating and is represented by the as-prepared data point at pH 1.8, seems to be a mixed oxide between V(IV) and V(V). After the as-prepared samples had been exposed to the higher pH environment of the gel coatings, the measured oxidation state decreased. For these samples, no potential was applied, so this transition occurred spontaneously. According to Fig. 2, the solid form most stable at pH 1.8 in the water stability region is the V(V) oxide, V_2O_5. However, at higher pH levels, the stable solid forms are the V(IV) and V(III) oxides, V_2O_4 and V_2O_3,

respectively. The increase in local pH seems to induce a reduction in vanadium oxidation state with subsequent K^+ intercalation for charge compensation. After cycling, the oxidation state seems to be approximately the same for pH 1.8, 5.0 and 7.5. The pH 5.0 and 7.5 samples were cycled in potential ranges where solid V(IV) and V(III) as well as dissolved V(V) species are most stable. Over the cycling, the vanadium may have transitioned to a lower oxidation state according to the more thermodynamically favorable state. However, the pH 1.8 environment was cycled in a potential range where solid V(V) and dissolved V(IV) and V(III) are stable. It is possible that over the course of cycling at pH 1.8, the oxide underwent irreversible reductive dissolution, and that dissolved species remaining on the surface were detected in the WDS measurement. The vanadium oxide cycled at pH 3.0 exhibited a much higher oxidation state than oxides cycled at other pHs, and higher than the oxidation state of the as-prepared sample before cycling. Thermodynamically, this pH and potential region correspond to the minimal solubility of the various solid oxide forms. The higher measured oxidation state could be due to either a relatively higher oxidation state of the solid form, or it could be due to residual dissolved species on the surface.

3.5. Morphological characterization using SEM

Although the electrochemical analysis points to dissolution as the mechanism responsible for degradation of capacitance, the morphology of the films was examined to determine whether cycle smoothing or surface area reduction upon cycling could also be a contributing factor. Fig. 15 shows secondary electron SEM images for the as-prepared samples, both vanadium oxide alone and oxides that had been coated with agar made with 1.0 M aqueous KCl at pH 3.0 and pH 6.0. The gel coating was allowed to set for a few minutes before removal. The nodular morphology of the vanadium oxide appeared to be unchanged by the agar deposition and removal procedure, but the size of the nodules appeared to increase with increasing pH of the agar.

A similar trend was observed for the images of the cycled samples reported in Fig. 16. These samples were all coated with approximately 400 μL, 1.0 M KCl agar and cycled in 1.0 M KCl at pH 1.8, 3.0, 5.0 or 7.5 by galvanostatic CD cycling before removing the agar and examining by SEM. As the pH increased, the nodular diameter also increased. This was especially noticeable between the pH 5.0 and 7.5 environments.

A coarser microstructure corresponds to a smaller active specific surface area, and thus the pseudocapacitive response would be reduced. This phenomenon could help to explain the behavior observed in Fig. 9, such as the initial increase in measured capacitance of the pH 1.8 sample. The morphology of the sample before and after cycling is represented by the SEM images in Figs. 15c and 16a, respectively. Fig. 16a indicates that exposure to pH 1.8 reduced the nodular diameter producing a larger surface area. The capacitance is directly related to the active surface area, thus an increase in surface area would increase the measured capacitance. The increase in nodular diameter with increasing pH might, at first sight, be attributed to Ostwald ripening, but this would not be

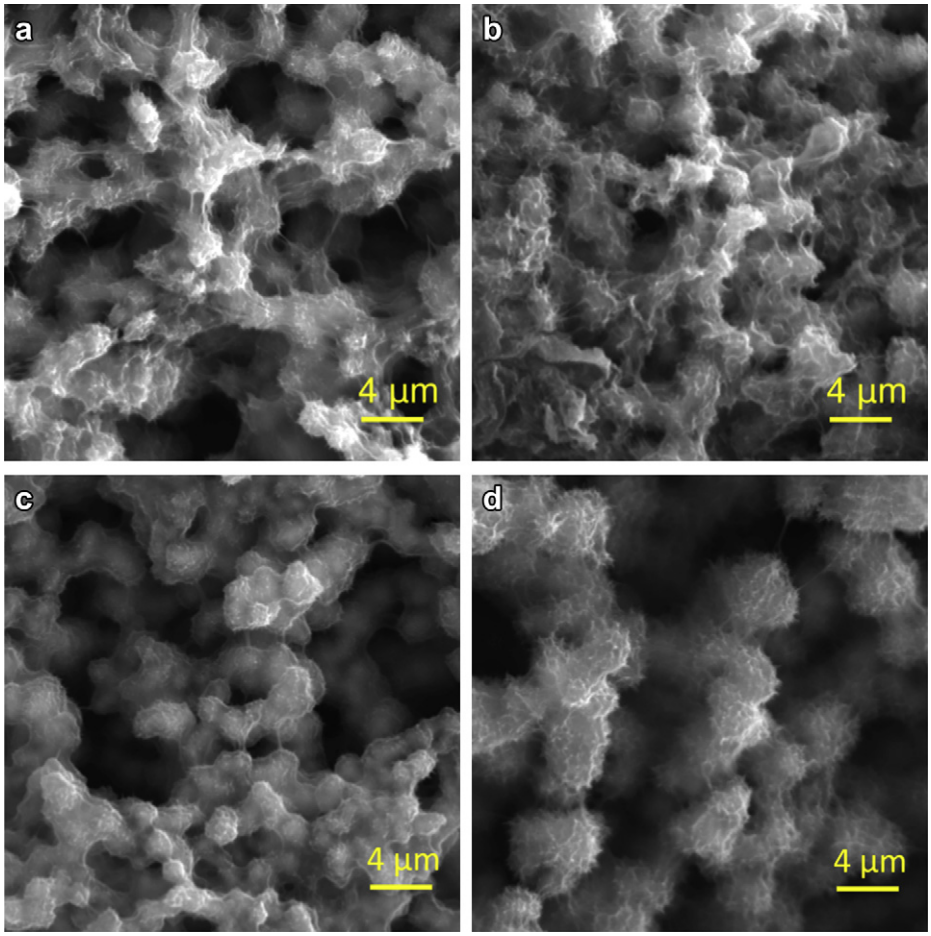

Fig. 16. Secondary electron images of vanadium oxide samples coated with approx. 400 μL 1.0 M KCl agar after thirty (30) ± 0.5 mA galvanostatic CD cycles in 1.0 M KCl at a) pH 1.8, b) pH 3.0, c) pH 5.0 and d) pH 7.5, followed by removal of the agar coatings using the testing electrolyte at approximately 100 °C.

reversible upon pH reduction. Perhaps, upon an increase in pH, an additional swelling is induced by K^+ intercalation, which may be reversible with decreasing pH. As cycling continues, oxide dissolution eventually dominates, which results in the sharp decrease in capacitance.

Also observed in Fig. 9 is the lower initial capacitance but longer cycle life of the oxide tested at pH 7.5 as compared to pH 5.0. Although this could reflect an innate characteristic of the slightly lower oxidation state demonstrated in the WDS results, it could also be due to the larger nodular size and reduced surface area for this environment. The lower surface area microstructure observed in the higher pH environment could in part explain the lower initial capacitance. Furthermore, the lower oxide–electrolyte interfacial area would decrease the rate of dissolution explaining the longer cycle life for the higher pH environment.

Lastly, when comparing the as-prepared and cycled morphologies, although the structure coarsens with increasing pH, it seems invariant upon cycling. A cycle smoothing effect does not seem to be occurring under the tested conditions. Therefore, the capacitive degradation mechanism does not seem to be significantly associated with microstructural change.

3.6. Degradation mechanisms in various aqueous environments

Both the electrochemical cycling data and the SEM morphological study support dissolution as the primary degradation mechanism responsible for reduced cycle life. Reductive dissolution to VO^{2+} in pH 1.8 was discussed in Section 3.1. However, this species is not the most stable dissolved species for every pH tested, as seen in Fig. 2. Fortuitously, the agar gel was transparent, making it easy to detect color changes due to dissolved species diffusing away from the electrode surface. Furthermore, the color of vanadium aquo ions depends on the oxidation state. Table 2 lists the thermodynamically favorable dissolved species for the various pHs in the potential ranges tested, the color of those dissolved species according to Ref. [18] and also the observed color of the gel during cycling.

By comparing the known color of dissolved species that are stable at some potential for a given pH with the observed color of the gel coating during cycling, those species that appear to predominate were identified. These are labeled with asterisks in Table 2. The blue-green color of the gel coating during cycling at pH 1.8 suggests reductive dissolution producing high concentrations of VO^{2+}, giving the blue color, and perhaps low activities of VO_2^+, known to be a light yellow color, or V^{3+}, which is green, which would give the additional greenish hue. The light yellow color observed in the pH 3.0 system supports oxidative dissolution to $H_3V_2O_7^-$, which is orange, but may appear yellow at low concentrations. The pH 5.0 system is similar to the pH 3.0 system with a yellow color, albeit more intense. This suggests that a higher concentration of $H_3V_2O_7^-$ was formed and moving through the gel. A dark brown-yellow color was observed during cycling in pH 7.5. This appears to be a combination of $H_3V_2O_7^-$, which diluted could add a yellow tint, $H_2VO_4^-$, which is thermodynamically stable but colorless, and $HV_2O_5^-$, which most likely provides the brown tint.

Table 2
Predominant dissolved species during cycling.

Solution pH	Dissolved species	V oxidation state	Solution color with dissolved ion [18]	Observed gel color during cycling
pH 1.8	VO_2^+	V	Light yellow	Blue-green
	$H_3V_2O_7^-$	V	Orange	
	$^*VO^{2+}$	IV	Blue	
	V^{3+}	III	Green	
pH 3.0	$^*H_3V_2O_7^-$	V	Orange	Light yellow
	VO^{2+}	IV	Blue	
	VOH^{2+}	III	Green	
	V^{3+}	III	Green	
pH 5.0	$^*H_3V_2O_7^-$	V	Orange	Yellow
	VO^{2+}	IV	Blue	
	$HV_2O_5^-$	IV	Red-brown	
	VO^+	III	Green	
pH 7.5	$^*H_3V_2O_7^-$	V	Orange	Dark brown-yellow
	$^*H_2VO_4^-$	V	Colorless	
	$^*HV_2O_5^-$	IV	Red-brown	
	VO^+	III	Green	

4. Conclusion

Electrodeposited vanadium oxide exhibits pseudocapacitive behavior well-suited for use in electrochemical capacitor electrodes. Unfortunately, it also presents a poor cycle life in aqueous systems due to dissolution upon cycling. Agar gel coatings have been used to control mass transport of the dissolved species, thereby lowering capacitive degradation in all pH environments tested. However, with or without the gel coating the vanadium oxide film tested in the 1.0 M KCl, pH 3.0 environment exhibited the best overall performance. Quantitative compositional analysis found that the vanadium oxidation state is depends somewhat on the pH, but dissolved species remaining on the surface of the electrode may have contributed to the apparent oxidation state. A study of the oxide morphology showed that the microstructure coarsened with increasing pH, which may partially explain the observed behavior that the oxides cycled at higher pH that exhibited a lower initial capacitance but a longer cycle life. Further study indicated that the microstructure did not change with cycling. Therefore, the electrochemical and characterization data indicate that the dominant mechanism for capacitive degradation is dissolution-related material loss, and the precise dissolved species produced during cycling depend on the pH of the testing electrolyte.

Acknowledgments

This material is based upon work supported by the National Science Foundation Graduate Research Fellowship under Grant No. DGE-1106400. Appreciation goes to Tim Teague for assistance with the SEM and EDS as well as to Sean Mulcahy for performing the WDS.

References

[1] B.E. Conway, Electrochemical Supercapacitors; Scientific Fundamentals and Technological Applications, Kluwer Academic/Plenum Publishers, New York, 1999.
[2] W. Deng, X. Ji, Q. Chen, C.E. Banks, RSC Adv. 1 (2011) 1171–1178.
[3] J.H. Chae, K.C. Ng, G.Z. Chen, J. Power Energ. 224A (2010) 479–503.
[4] H.Y. Lee, J.B. Goodenough, J. Solid State Chem. 148 (1999) 81–84.
[5] Y. Sato, T. Nomura, H. Tanaka, K. Kobayakawa, J. Electrochem. Soc. 138 (1991) L37–L39.
[6] E. Shembel, R. Apostolova, V. Nagirnyi, D. Aurbach, B. Markovsky, J. Power Sources 81 (1999) 480–486.
[7] E. Potiron, A.L. La Salle, A. Verbaere, Y. Pifard, D. Guyomard, Electrochim. Acta 45 (1999) 197–214.
[8] P. Liu, J.G. Zhang, C.E. Tracy, J.A. Turner, Electrochem. Solid State Lett. 3 (4) (2000) 163–166.
[9] M. Nakayama, A. Tanaka, S. Konishi, K. Ogura, J. Mater. Res. 19 (2004) 1509–1515.
[10] K. Takahashi, S.J. Limmer, Y. Wang, G.Z. Cao, J. Phys. Chem. B 108 (28) (2004) 9795–9800.
[11] V.M. Nagirnyi, R.D. Apostolova, E.M. Shembel, Russ. J. Appl. Chem. 79 (2006) 1443–1446.
[12] I.H. Kim, J.H. Kim, B.W. Cho, K.B. Kim, J. Electrochem. Soc. 153 (2006) A1451–A1458.
[13] D.L. da Silva, R.G. Delatorre, G. Pattanaik, G. Zangari, W. Figueiredo, R. Blum, H. Niehus, A.A. Pasa, J. Electrochem. Soc. 155 (2008) E14–E17.
[14] C. Huang, C. Hu, K. Chang, J. Li, Y. Li, J. Electrochem. Soc. 156 (8) (2009) A67–A671.

[15] H. Jeon, B. Jeong, J.K. Lee, H.S. Kim, S. Lee, J. Lee, Electrochem. Solid State Lett. 13 (3) (2010) A25–A28.
[16] S. Chou, J. Wang, H. Liu, S. Dou, Adv. Sci. Lett. 3 (2010) 295–298.
[17] P. Pande, P. Rasmussen, L. Thompson. ECS Meeting. Las Vegas, NV, Oct. 13, 2010.
[18] M. Pourbaix, Atlas of Electrochemical Equilibria in Aqueous Solutions, second ed., National Association of Corrosion Engineers, Houston, 1974, pp. 234–245.
[19] E. Muthuswamy, S.S. Ramadevi, H.N. Vasan, C. Garcia, L. Noe, M. Verelst, J. Nanoparticle Res. 9 (2007) 561–567.
[20] M. Lahaye, J. Appl. Phycol. 13 (2001) 173–184.
[21] C.M.A. Brett, A.M.O. Brett, Electrochemistry: Principles, Methods, and Applications, Oxford, Oxford UP, 1993, pp. 341–345.
[22] J. Chang, J. Park, Y.K. Pak, J.J. Pak, Neural engineering, in: 2007 CNE '07 3rd International IEEE/EMBS Conference on Neural Engineering 2007, pp. 572–574.